On the Comprehensive Kinematics Analysis of a Humanoid Parallel Ankle Mechanism

Chengxu Zhou*
Humanoid and Human Centered Mechatronics Research Line
Istituto Italiano di Tecnologia
via Morego, 30, 16163 Genova, Italy.
Email: zhouchengxu@gmail.com

Nikos Tsagarakis
Humanoid and Human Centered Mechatronics Research Line
Istituto Italiano di Tecnologia
via Morego, 30, 16163 Genova, Italy.
Email: nikos.tsagarakis@iit.it

ABSTRACT

In this paper we present a thorough kinematics analysis of a humanoid two degrees of freedom (DoF) ankle module based on a parallel kinematics mechanism. Compared with the conventional serial configuration, the parallel kinematics ankle permits the distribution of the torque/power of the actuators to the two DoF of the ankle taking full advantage of available power/torque capacity of the two actuators. However, it complicates the kinematics study in return. In this work a complete study of a parallel ankle mechanism is performed that permits the full characterization of the ankle module for the purpose of its design study, control and performance evaluation. Screw theory is employed for mobility analysis to firstly determine the number and properties of the mechanism's DoFs. Then the inverse kinematics is solved analytically and the Jacobian matrix for describing the velocity relation between the ankle joints and motors is found. Based on these results, the forward kinematics of the parallel mechanism can be numerically computed using the Newton-Raphson method. The workspace of the ankle is also analyzed and the motor limits are decided accordingly. Finally, an experimental demonstration consisting of four tests is carried out to evaluate the proposed methods and ankle module.

1 Introduction

A typical parallel mechanism is defined as such that a mechanism has two or more serial kinematic chains connecting a moving platform to a fixed base. Parallel mechanisms can offer advantages over their serial companions in terms of rigidity, accuracy, dynamic performance and ability to distribute the torque/power of the actuators to the degree of freedom (DoF) of the mechanism. Apart from their extensive use in automation, parallel mechanisms also attract considerable attention from the humanoid robotics community due to these advantages.

In [1], a humanoid robotic shoulder complex which is composed by a parallel mechanism and a serial mechanism was presented and the kinematics of humanoid humeral pointing were performed by this complex. A fully decoupled parallel wrist has been also developed taking the advantages of both parallel mechanism and decoupled motion [2]. Morisawa *et al*. [3] studied bipedal motion on a robot which has three identical parallel 6-DoF limbs of each leg. Hashimoto *et al*. [4] developed a human-carrying walking vehicle which has two parallel kinematics legs. Parallel mechanisms are also popular in human ankle rehabilitation research. ARBOT [5] adopted a redundantly actuated parallel mechanism which is capable of delivering the required forces and torques needed for ankle strengthening and balance exercises. MIT's Anklebot [6], which has proven its potential to evoke positive changes for chronic stroke patients, is an underactuated 3-DoF ankle rehabilitation device with only two parallel mounted actuators.

Regarding the ankle of a humanoid robot, which usually consists of one roll joint and one pitch joint, previous study [7] has compared the torque profile difference between serial and parallel configurations for the actuators of these two joints. If

*Corresponding author.

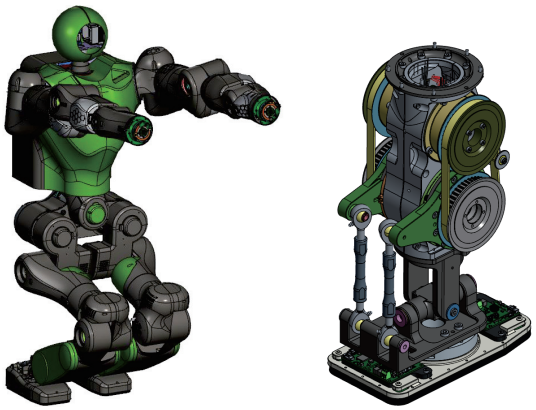

Fig. 1: Mechanical model of the CogIMon humanoid robot (left) and close back view of its tibia without covers (right).

the ankle joints are placed in series, the pitch actuator requires more power than the roll one. In contrast, both actuators can be identical and with smaller size when they are placed in a parallel manner because the loads can be distributed evenly if needed.

Moreover, a parallel ankle will also have the actuators placed away from the ankle joint, which reduces the inertia of the tibia and improves the dynamic behavior during walking leg swing, thereby reducing power consumption. On the other hand, parallel mechanism allows large output torque at the price of narrower range of joint motion. Despite these benefits, they also represent more complex mechanisms from the kinematics analysis point of view, therefore requiring more extensive study to derive their specifications during the robot design process or subsequently to control and evaluate their performance.

Due to the intrinsic property of linear actuation, most of the humanoid robots powered by the conventional hydraulic linear actuators ended up with a parallel ankle design. The hydraulic humanoid robots TaeMu [8] simply applied a differential relation to the two coupled ankle joints, Atlas [9] resolved the ankle actuator commands based on the ankle joint velocities and Hydra [10] had a closed form solution for inverse kinematics and the Jacobian matrix was also derived.

Several humanoid robots powered by electrical actuators make also use of the parallel mechanism to realize their ankle modules. Lola [7], ESCHER [11] and RHP2's [12] ankles used two identical ball-screw drives in parallel as length-variable steering rods. DURUS developed by SRI International [13] added springs to make its parallel actuated ankle passive compliant to further improve the energy efficiency. STEPPR and WANDERER developed by Sandia National Laboratories [14] developed parallel springs in addition to their parallel designed ankle for the same purpose. Similarly to the design of STEPPR, in which the two parallel rods were placed in the frontal side, the G-robot developed at KAIST [15] considered directly a linear kinematic relation between the joints and motors, which is only true when the roll angle is relatively small. A new parallel ankle design with three DoFs has been also developed for humanoid robots in [16]. However, none of these works have provided a detailed kinematics study of their ankle parallel designs, which motivates us to conduct the work of this paper.

The main contribution of this work is a comprehensive thorough investigation on the kinematic properties and characterization of an ankle parallel mechanism for the benefit of the humanoids and, in general, the robotics community. The work presents an all-inclusive study of a parallel ankle module that provides the necessary foundation to study such joints as part of the robot design process or to derive the necessary kinematics formulations required to subsequently control the parallel ankle module under different control modes including position, velocity and torque approaches

In particular, we performed the kinematics analysis for the parallel actuated ankle of the under development humanoid robot CogIMon[1] as shown in the left figure of Fig. 1. CogIMon is aiming at advancing the cognitive interactions between human and/or robots in real world scenarios. Its ankle configuration employs two actuators in a parallel arrangement as shown in the right figure of Fig. 1.

The rest of the work is organized as follows. Section 2 introduces the kinematics design of the ankle parallel mechanism as well as the mobility analysis performed using screw theory. In Section 3, the analytic inverse kinematics and Jacobian analysis are derived. Subsequently, the forward kinematics is computed numerically based on the previous results. The workspace of the designed mechanism is finally studied. Section 4 experimentally demonstrates the developed kinematics solvers' performances with practical trajectories. We summarize and conclude this work in Section 5.

Journal of Mechanisms and Robotics. Received October 23, 2017;
Accepted manuscript posted July 17, 2018. doi:10.1115/1.4040886

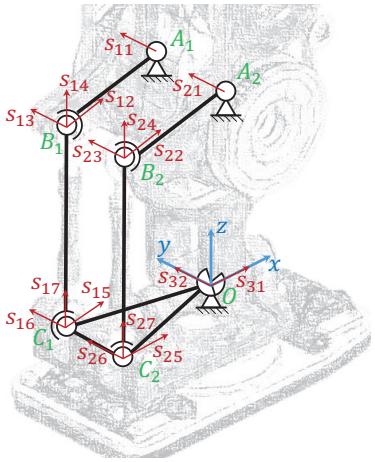

Fig. 2: The ankle's schematic representation.

2 Mechanism Description and Motion Analysis

2.1 Description of the Ankle Mechanism

As shown in the right part of Fig. 1, the humanoid robot CogIMon's ankle consists of a parallel 2-RSS-1-U[2] mechanism and a moving platform (the foot). The schematic representation of ankle is shown in Fig. 2. This parallel mechanism has 7 joints in total, which are 2 hinge joints ($A_{1,2}$), 1 universal joint (O) and 4 ball joints ($B_{1,2}, C_{1,2}$). There are three kinematic chains connecting the fixed base (tibia) and the foot, called limb 1 ($A_1B_1C_1$), limb 2 ($A_2B_2C_2$) and limb 3 (O), where limb 3 has only one joint O and limb 1 and 2 consist of two links and three joints, respectively.

When the foot is in its initial configuration, the foot is perpendicular to the tibia and the two motors are in zero position. We place the base frame at the center of the universal joint O, with its positive x-axis pointing in the forward direction as shown in Fig. 2, positive z-axis points upwards along the tibia, and y-axis follows the right-handed coordinates. This base frame is fixed and does not move together with the foot. For the rest of the paper, all the variables are defined in this base frame if there is no additional explanations.

Each joint has its own local frame located in the joint center and the coordinate axes initially point to the same directions of the base frame. Therefore, as shown in the right part of Fig. 1, the universal joint O's two rotational axes are about x_O- and y_O-axis, the x- and y-axis of its local frame, respectively. The orientation of y_O-axis in the base frame will never change since it is mechanically fixed to the tibia. On the contrary, the orientation of x_O-axis in the base frame varies with the joint O's rotation angle about y_O-axis.

A position vector $\boldsymbol{r}_{jnt}$ is defined as a vector represented in the base frame originated from joint O to the joint jnt. Therefore, the designed dimensions of each link of the proposed ankle module are represented as follows,

$$
\begin{aligned}
l_{bar} &= \|{}^0\boldsymbol{r}_{B_i} - {}^0\boldsymbol{r}_{A_i}\| = \{{}^0\boldsymbol{r}_O - {}^0\boldsymbol{r}_{C_i}\}_x = \ 85 \ \text{mm}, \\
l_{rod} &= \|{}^0\boldsymbol{r}_{C_i} - {}^0\boldsymbol{r}_{B_i}\| = \{{}^0\boldsymbol{r}_O - {}^0\boldsymbol{r}_{A_i}\}_z = \ 135 \ \text{mm}, \\
l_{spacing} &= \|{}^0\boldsymbol{r}_{A_1} - {}^0\boldsymbol{r}_{A_2}\| = \|{}^0\boldsymbol{r}_{B_1} - {}^0\boldsymbol{r}_{B_2}\| = \|{}^0\boldsymbol{r}_{C_1} - {}^0\boldsymbol{r}_{C_2}\| = \ 43 \ \text{mm},
\end{aligned}
$$

where the vector with a left superscript zero represents the vector in initial foot configuration, the operator $\{\cdot\}$ represents the element of a vector.

Instead of the widely used UPU[3] or UPS limbs (such as in the robots developed in [7, 8, 9, 10, 11, 12]), we adopt the RSS limb to the proposed parallel mechanism not only for the benefit of the doubled output torque from the parallel mechanism, but also for a constant torque transmission within the range of motion of the ankle joint. In a UPU or UPS limbed parallel ankle mechanism, the maximum torque that the ankle joint could provide is nonlinear, it depends on the mechanism configuration and is significantly reduced when the foot rotates away from its initial position, which is not a preferable feature of a humanoid ankle. In contrast, in a RSS limbed one, the transmission, that between the actuator output (about y_{A_i}-axis) and the pitch component of the torque (about y_O-axis) that the actuator applied to the joint, is independent of the mechanism configuration.

[1] Cognitive Interaction in Motion, `https://cogimon.eu`
[2] R, S, and U stand for revolute, spherical, and universal joint, respectively. The underlined letter represents the actuated joint.
[3] P stands for prismatic joint.

2.2 Mobility Analysis

The mobility analysis is important for better understanding the motion capabilities of the parallel mechanism. The Grübler-Kutzbach criterion [17] is a useful tool for mobility analysis, however, it has the drawback that only the mechanism's DoF number can be derived, while the properties of the DoFs remain unknown, i.e. whether they are translational or rotational. In contrast, we can effectively analyze the mobility of a parallel mechanism, both the number of the DoFs and their axes using screw theory.

A uniti screw $\$$ is an element in a six-dimensional linear vector space with transformation properties [18, 19], defined as

$$\$ = (\boldsymbol{s}; \boldsymbol{s}_o) = (\boldsymbol{s}; \boldsymbol{r} \times \boldsymbol{s} + p\boldsymbol{s}), \tag{1}$$

where $\boldsymbol{s}$ is a unit vector represents screw axis direction, $\boldsymbol{r}$ is the position vector of any point on the screw axis in terms of a reference coordinate system, and p is called the pitch.

Two screws are reciprocal if they satisfy the following condition

$$\$ \circ \$^r = \boldsymbol{s} \cdot \boldsymbol{s}_o^r + \boldsymbol{s}^r \cdot \boldsymbol{s}_o = 0, \tag{2}$$

where the operator $\circ$ represents the reciprocal product.

A screw system $\hat{\boldsymbol{S}}$ is a set of screws. Therefore, its reciprocal screw set $\hat{\boldsymbol{S}}^r$ is defined by

$$\hat{\boldsymbol{S}}^r \equiv \{\$^r | \$ \circ \$^r = 0, \forall \$ \in \hat{\boldsymbol{S}}\}, \tag{3}$$

and the sum of the ranks of a screw system and its reciprocal is always six, i.e. $rank(\hat{\boldsymbol{S}}) + rank(\hat{\boldsymbol{S}}^r) = 6$. Therefore, when $rank(\hat{\boldsymbol{S}}) = 6$, there exists no reciprocal screws. If $rank(\hat{\boldsymbol{S}}) < 6$, then $rank(\hat{\boldsymbol{S}}^r) = 6 - rank(\hat{\boldsymbol{S}})$, which indicates that there are $rank(\hat{\boldsymbol{S}}^r)$ linearly independent constraints to the screw system.

For a parallel mechanism, if all the joints' DoFs are defined by unit screws $\$_{ij}$, where i is the limb name, j is the joint's DoF order of a limb, the motion of each limb can be represented as a screw system $\hat{\boldsymbol{S}}_i$ under some structural constraints $\hat{\boldsymbol{S}}_i^r$.

For the proposed parallel mechanism, its unit vectors $\boldsymbol{s}_{ij}$ of $\$_{ij}$ are defined and shown in Fig. 2. Therefore, the screw system representing the DoFs of limb 3, which has only one universal joint, is defined as

$$\hat{\boldsymbol{S}}_3 = \begin{cases} \$_{31} = (\boldsymbol{s}_{31}; \boldsymbol{r}_O \times \boldsymbol{s}_{31}) \\ \$_{32} = (\boldsymbol{s}_{32}; \boldsymbol{r}_O \times \boldsymbol{s}_{32}) \end{cases} \tag{4}$$

where $\boldsymbol{s}_{31} = (\cos\alpha \; 0 \; -\sin\alpha)$, $\boldsymbol{s}_{32} = (0 \; 1 \; 0)$ and $\boldsymbol{r}_O = (0 \; 0 \; 0)$, α is the joint O's rotation angle about y_o-axis.

Thus the constraint screw system of limb 3 is

$$\hat{\boldsymbol{S}}_3^r = \begin{cases} (1\;0\;0;\; 0\;0\;0) \\ (0\;1\;0;\; 0\;0\;0) \\ (0\;0\;1;\; 0\;0\;0) \\ (0\;0\;0;\; \sin\alpha\; 0\; \cos\alpha) \end{cases}. \tag{5}$$

Correspondingly, the screw sets of limb 1 and 2 can be written as

$$\hat{\boldsymbol{S}}_i = \begin{cases} \$_{i1} = (\boldsymbol{s}_{i1}; \boldsymbol{r}_{A_i} \times \boldsymbol{s}_{i1}) \\ \$_{i2} = (\boldsymbol{s}_{i2}; \boldsymbol{r}_{B_i} \times \boldsymbol{s}_{i2}) \\ \$_{i3} = (\boldsymbol{s}_{i3}; \boldsymbol{r}_{B_i} \times \boldsymbol{s}_{i3}) \\ \$_{i4} = (\boldsymbol{s}_{i4}; \boldsymbol{r}_{B_i} \times \boldsymbol{s}_{i4}) \\ \$_{i5} = (\boldsymbol{s}_{i5}; \boldsymbol{r}_{C_i} \times \boldsymbol{s}_{i5}) \\ \$_{i6} = (\boldsymbol{s}_{i6}; \boldsymbol{r}_{C_i} \times \boldsymbol{s}_{i6}) \\ \$_{i7} = (\boldsymbol{s}_{i7}; \boldsymbol{r}_{C_i} \times \boldsymbol{s}_{i7}) \end{cases}, \quad for\ i = 1, 2. \tag{6}$$

It is straightforward to find out that the ranks of these screw sets are 6, which means that the reciprocal screw sets $\hat{\boldsymbol{S}}^{r}_{1,2}$ are empty, that is, limb 1 and 2 provide no constraints to the foot motion. Hence, the motion screw set of the foot $\hat{\boldsymbol{S}}_{ft}$, which is the reciprocal screw set of the union of three limbs' constraint screw sets [20], can be obtained as

$$\hat{\boldsymbol{S}}_{ft} = (\cup_{i=1}^{3} \hat{\boldsymbol{S}}_i^{r})^{r} = (\hat{\boldsymbol{S}}_3^{r})^{r} = \begin{cases} (\cos\alpha\ 0\ -\sin\alpha;\ 0\ 0\ 0) \\ (0\ 1\ 0;\ 0\ 0\ 0) \end{cases}, \tag{7}$$

which indicates that, the foot has two rotational DoFs which are perpendicular with each other. One revolution DoF is around the y-axis, and the other's rotational axis is dependent on α. They are exactly the two rotational axes of the universal joint O, x_O- and y_O-axis, represented in the base frame.

3 Kinematics Analysis

In this section, we study the kinematic relations between the parallel ankle joints and actuators. As shown in Fig. 3, the derived kinematics solvers will be integrated into our locomotion framework [21] for realizing dynamic walking and balancing motions. Due to the features of the parallel ankle design, the outputs of leg inverse kinematics [22] could not be sent to the leg actuators directly. The ankle inverse kinematics needs to be resolved first to derive the motor commands $\boldsymbol{\theta}$ taking the ankle joint references $\boldsymbol{q}_{ankle}$ generated by the leg inverse kinematics as input. On the other hand, the ankle motor sensors feedback $\boldsymbol{\theta}^{m}$ also need to be firstly converted to the ankle joint angles $\boldsymbol{q}^{m}_{ankle}$ by the ankle forward kinematics before sending them to, for example, the robot center of mass state estimator [21].

3.1 Ankle Inverse Kinematics

The inverse kinematics problem resolves the actuated variables $\boldsymbol{\theta}$ from a given pose $\boldsymbol{x}$ (position and orientation) of the foot and is represented as follows,

$$\boldsymbol{\theta} = f_{ik}(\boldsymbol{x}), \tag{8}$$

where $\boldsymbol{\theta} = [\theta_1; \theta_2]$ is the position vector of the two actuators, $\boldsymbol{x}$ is the pose of the foot in base frame, whose translational part $\boldsymbol{x}_{trans} \in \mathbb{R}^3$ is $\boldsymbol{r}_O$ and rotational part $\boldsymbol{x}_{rot} \in \mathbb{R}^{3\times3}$ is constrained only to roll and pitch rotations revealed by Eqn. 7, the subscript "*ik*" stands for "inverse kinematics".

Considering the schematic presented in Fig. 2, the following relations hold for limb 1 and 2 at any configurations,

$$\|\boldsymbol{r}_{C_i} - \boldsymbol{r}_{B_i}\| = l_{rod}\ , \quad for\ i = 1, 2, \tag{9}$$

where

$$\begin{aligned} \boldsymbol{r}_{B_i} &= \boldsymbol{r}_{A_i} + \boldsymbol{R}_y(\theta_i)({}^{0}\boldsymbol{r}_{B_i} - {}^{0}\boldsymbol{r}_{A_i}), \\ \boldsymbol{r}_{C_i} &= \boldsymbol{x}_{rot}\,{}^{0}\boldsymbol{r}_{C_i}, \\ \boldsymbol{r}_{A_i} &= {}^{0}\boldsymbol{r}_{A_i}, \end{aligned}$$

$\boldsymbol{R}_y(\theta_i) \in \mathbb{R}^3$ is the basic rotation matrix about y-axis by an angle θ_i.

Therefore, by solving Eqn. 9, the motor positions can be obtained as follows,

$$\theta_i = \arcsin\left(\frac{bc + \sqrt{b^2c^2 - (a^2+b^2)(c^2-a^2)}}{(a^2+b^2)}\right), \tag{10}$$

where

$$\begin{aligned} a &= \{\boldsymbol{r}_{C_i} - \boldsymbol{r}_{A_i}\}_x, \\ b &= \{\boldsymbol{r}_{A_i} - \boldsymbol{r}_{C_i}\}_z, \\ c &= \frac{l_{rod}^2 - l_{bar}^2 - \|\boldsymbol{r}_{C_i} - \boldsymbol{r}_{A_i}\|^2}{2l_{bar}}. \end{aligned}$$

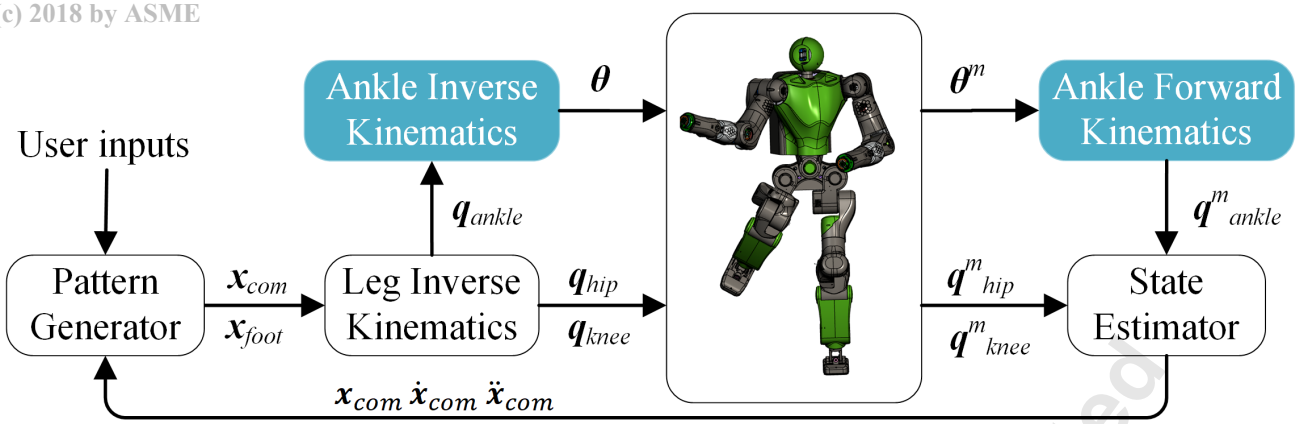

Fig. 3: Typical Control Framework for humanoid motion control. The superscript m indicates the variable is measured by the sensors.

As presented in Fig. 3, after integrating the ankle inverse kinematics Eqn. 8 into the locomotion framework, instead of the foot pose references, it actually needs to take the ankle joint position references ($\boldsymbol{q}_{ankle}$ in Fig. 3) as inputs. Therefore, we define $\boldsymbol{x}_c = [q^{roll}_{ankle}; q^{pitch}_{ankle}]$ as the constrained (reduced) position variable, where q^{roll}_{ankle} and q^{pitch}_{ankle} are the ankle roll and pitch joint rotations, respectively, and the foot rotation in base frame can be calculated as follows,

$$\boldsymbol{x}_{rot} = \boldsymbol{R}_y(q^{pitch}_{ankle})\boldsymbol{R}_x(q^{roll}_{ankle}). \tag{11}$$

Therefore, the inverse kinematics Eqn. 8 can also be represented by the constrained position variable as

$$\boldsymbol{\theta} = f_{ik}(\boldsymbol{x}_c). \tag{12}$$

3.2 Jacobian Matrix

Let $\boldsymbol{r}_{bar_i} = \boldsymbol{r}_{B_i} - \boldsymbol{r}_{A_i}$ and $\boldsymbol{r}_{rod_i} = \boldsymbol{r}_{C_i} - \boldsymbol{r}_{B_i}$, from Fig. 2, we can have the following relations for limb 1 and 2,

$$\boldsymbol{r}_{C_i} = \boldsymbol{r}_{A_i} + \boldsymbol{r}_{bar_i} + \boldsymbol{r}_{rod_i}. \tag{13}$$

Let $\dot{\boldsymbol{\theta}} = [\dot{\theta}_1; \dot{\theta}_2] \in \mathbb{R}^2$ be the velocity vector of the two motors located at A_1 and A_2, respectively, $\dot{\boldsymbol{x}} = [\boldsymbol{v}; \boldsymbol{\omega}] \in \mathbb{R}^6$ be the velocity vector of the foot, where $\boldsymbol{v} = \dot{\boldsymbol{r}}_O$ is the translational velocity of the center of joint O connected to the foot, $\boldsymbol{\omega}$ is the angular velocity of the foot. By differentiating Eqn. 13 with respect to time yields

$$\boldsymbol{v} + \boldsymbol{\omega} \times \boldsymbol{r}_{C_i} = \dot{\theta}_i \boldsymbol{s}_{i1} \times \boldsymbol{r}_{bar_i} + \boldsymbol{\omega}_{rod_i} \times \boldsymbol{r}_{rod_i}, \tag{14}$$

where $\boldsymbol{\omega}_{rod_i}$ is the angular velocity of the rod, which can be eliminated by multiplying Eqn. 14 by $\boldsymbol{r}_{rod_i}$. Therefore, the previous equation yields to

$$\boldsymbol{r}_{rod_i} \cdot \boldsymbol{v} + \boldsymbol{\omega} \cdot (\boldsymbol{r}_{C_i} \times \boldsymbol{r}_{rod_i}) = \dot{\theta}_i \boldsymbol{s}_{i1} \cdot (\boldsymbol{r}_{bar_i} \times \boldsymbol{r}_{rod_i}). \tag{15}$$

The following equation can be derived from Eqn. 15,

$$\boldsymbol{J}_x \dot{\boldsymbol{x}} = \boldsymbol{J}_\theta \dot{\boldsymbol{\theta}}, \tag{16}$$

with

$$\boldsymbol{J}_x = \begin{bmatrix} \boldsymbol{r}^T_{rod_1} & (\boldsymbol{r}_{C_1} \times \boldsymbol{r}_{rod_1})^T \\ \boldsymbol{r}^T_{rod_2} & (\boldsymbol{r}_{C_2} \times \boldsymbol{r}_{rod_2})^T \end{bmatrix} \in \mathbb{R}^{2\times 6},$$

$$\boldsymbol{J}_\theta = \begin{bmatrix} \boldsymbol{s}_{11} \cdot (\boldsymbol{r}_{bar_1} \times \boldsymbol{r}_{rod_1}) & 0 \\ 0 & \boldsymbol{s}_{21} \cdot (\boldsymbol{r}_{bar_2} \times \boldsymbol{r}_{rod_2}) \end{bmatrix} \in \mathbb{R}^{2\times 2}.$$

The determinant of $\boldsymbol{J}_\theta$ equals zero indicates the inverse kinematics singularity, and a forward kinematic singularity occurs when $\boldsymbol{J}_x$ is not full rank.

When the mechanism is away from singularity, we have

$$\dot{\boldsymbol{\theta}} = \boldsymbol{J}\dot{\boldsymbol{x}}, \tag{17}$$

where $\boldsymbol{J} = \boldsymbol{J}_\theta^{-1}\boldsymbol{J}_x \in \mathbb{R}^{2\times 6}$ is the Jacobian matrix, which is, by convention, the inverse of the serial mechanisms'.

Based on the results from Section 2.2, the proposed parallel mechanism is constrained to only two rotational motions about x_O- and y_O-axis. Therefore, let $\dot{\boldsymbol{x}}_c = [\dot{q}^{roll}_{ankle}; \dot{q}^{pitch}_{ankle}]$, the ankle joints velocities, be the new constrained (reduced) velocity variable, we have

$$\dot{\boldsymbol{x}} = \boldsymbol{G}\dot{\boldsymbol{x}}_c, \tag{18}$$

where

$$\boldsymbol{G} = \begin{bmatrix} 0 & 0 & 0 & \cos\alpha & 0 & -\sin\alpha \\ 0 & 0 & 0 & 0 & 1 & 0 \end{bmatrix}^T \in \mathbb{R}^{6\times 2},$$

α is the joint O's rotation angle about y_O-axis, that is q^{pitch}_{ankle}.

Therefore, we can rewrite Eqn. 17 to

$$\dot{\boldsymbol{\theta}} = \boldsymbol{J}_c\dot{\boldsymbol{x}}_c, \tag{19}$$

where $\boldsymbol{J}_c = \boldsymbol{J}\boldsymbol{G} \in \mathbb{R}^{2\times 2}$ is the constrained Jacobian matrix which imposes the effect of the mechanical constraints on the mechanism.

3.3 Ankle Forward Kinematics

Given a set of motor position inputs, the pose of the foot needs to be resolved by the forward kinematics, which can also be presented by the constrained position variable as follows

$$\boldsymbol{x}_c = f_{fk}(\boldsymbol{\theta}_{ref}), \tag{20}$$

the subscript "*fk*" stands for "forward kinematics".

The same condition Eqn. 9 holds for solving Eqn. 20, however, analytically solving this would require to solve a high order polynomial function. For instance, using the Bezout's elimination method, Tsai *et al*. [23] solved a 16^{th} order polynomial to obtain the moving platform's pose of a 3-PRS parallel mechanism, also additional considerations were needed to select the final preferred solution among many solutions. Therefore, to avoid convoluted computation, the Newton-Raphson method is used in this work to solve the forward kinematics numerically.

For given motor references $\boldsymbol{\theta}_{ref}$, the resolved foot pose $\boldsymbol{x}_c$ should satisfy the following relation,

$$f_{err}(\boldsymbol{x}_c) = f_{ik}(\boldsymbol{x}_c) - \boldsymbol{\theta}_{ref} = 0. \tag{21}$$

Let $\boldsymbol{x}_c^k$ be the k^{th} iteration's solution, then the following equation is used to find successively the approximations to the roots of Eqn. 21,

$$\boldsymbol{x}_c^{k+1} = \boldsymbol{x}_c^k - \left(\frac{\partial f_{err}(\boldsymbol{x}_c^k)}{\partial \boldsymbol{x}_c^k}\right)^{-1} f_{err}(\boldsymbol{x}_c^k), \tag{22}$$

substituting $\frac{\partial f_{err}(\boldsymbol{x}_c^k)}{\partial \boldsymbol{x}_c^k} = \boldsymbol{J}_c(\boldsymbol{x}_c^k)$, Eqn. 12 and Eqn. 21 to Eqn. 22, yields

$$\boldsymbol{x}_c^{k+1} = \boldsymbol{x}_c^k - (\boldsymbol{J}_c(\boldsymbol{x}_c^k))^{-1}(f_{ik}(\boldsymbol{x}_c^k) - \boldsymbol{\theta}_{ref}). \tag{23}$$

Table 1: Example of solving the forward kinematics using Newton-Raphson method (unit: degree), the motor references are $[-46.38490723; -53.91584432]$ degree.

Iter.	q_{ankle}^{roll}	q_{ankle}^{pitch}	θ_1	θ_2
0	0	0	0	0
1	14.88673610	-50.15037578	-46.56169296	-54.03686823
2	14.99997178	-49.99999958	-46.38491322	-53.91583635
3	15.00000000	-50.00000000	-46.38490723	-53.91584432

Table 2: The workspace changes w.r.t the linkage dimensions according to Fig. 4.

Increasing only the	l_{bar}	l_{rod}	$l_{spacing}$
Workspace	Increased	Almost Same	Decreased

Thus, to solve the foot orientation from a given set of the motor positions $\boldsymbol{\theta}_{ref}$, the process of the Newton-Raphson iteration firstly starts with an initial guess of the constrained position variable $\boldsymbol{x}_c^{init}$, and will be terminated once the maximum absolute value of the error Eqn. 21 is less than a predefined threshold σ, where $1e^{-6}$ degree is used in this study.

To analyze the performance of the forward kinematics, we firstly let the foot be in the Cartesian pose represented by the constrained position variable $[q_{ankle}^{roll}; q_{ankle}^{pitch}] = [15; -50]$ degree. Then, by solving the inverse kinematics Eqn. 12, the corresponding motor positions are $[\theta_1; \theta_2] = [-46.38490723; -53.91584432]$ degree, which will be used as the motor position reference $\boldsymbol{\theta}_{ref}$ in Eqn. 20.

Therefore, as shown in Table 1, to find the foot orientation, the Newton-Raphson iteration started with initial guess $\boldsymbol{x}_c^{init} = [0; 0]$ degree, and the convergence was reached after just three iterations. It can be seen that the results converged very fast after even one iteration, by choosing properly the initial guess $\boldsymbol{x}_c^{init}$, such as an intuitive guess of a given motor configuration or the previous pose while executing a trajectory, the whole process will be accelerated even more and converges to the solution within just one iteration.

3.4 Workspace Analysis

Due to the properties of the parallel mechanism, the kinematic relation between the ankle joints and motors is not straightforward, therefore, it is essential to study the ankle workspace and investigate how the mechanism geometry and the motor limits could potentially affect this workspace.

First, we analyze the workspace considering only the geometric structure of the mechanism. By neglecting the possible physical collisions between the links and assuming that the two parallel kinematic chains, limb 1 and 2, have the same dimensions and symmetrically placed, the workspace of the proposed ankle module is solely determined by three parameters, the motor bar length l_{bar}, the rod length l_{rod} and the spacing between the two rods $l_{spacing}$.

Fig. 4 qualitatively demonstrates the workspace's changes w.r.t the previously mentioned three dimensions l_{bar}, l_{rod} and $l_{spacing}$. The area in green is the workspace of $l_{bar} = l_{rod} = l_{spacing}$ and is shown as a benchmark. We then respectively increase the three parameters to five times of their original length, and the corresponding workspaces are shown in different colors. By only increasing l_{bar}, the workspace increases to the blue area. By only increasing $l_{spacing}$, the workspace significantly decreases to the yellow area. Finally, if l_{rod} only increases, the workspace does not change much but it only shifts as shown in pink area. Note that, due to the intrinsic characteristics of the parallel mechanism, the roll and pitch limits are coupled therefore the workspace is not a rectangular area. The influences of each parameter variation to the workspace are summarized in Table 2, which indicates that, to obtain a large workspace, the geometry of the mechanism should be designed with as longer l_{bar} and narrower $l_{spacing}$ as possible. Meanwhile, the l_{rod} could be selected for proper desired workspace. By additionally considering the mechanical feasibilities and available volume and size of the tibia/ankle module, we conclude to the sizing of these parameters as follows, $l_{bar} = 85$ mm, $l_{rod} = 135$ mm and $l_{spacing} = 43$ mm.

Under the constraints of the above-mentioned linkage dimensions, especially the limited motion range of the rod end bearing, which affects significantly the ankle roll motion, the ankle joints limits were set to [-20, 20] degree for roll joint and [-58, 42] for pitch joint, which is shown as the red dashed box in Fig. 5. As mentioned previously, the ankle roll and pitch limits are coupled in a parallel mechanism, therefore the motor limits could not be defined straightforwardly as those of serial mechanism. As shown in Fig. 5, the parameter scan of the motor limits is done to find out the minimum workspace that contains the desired workspace (the red dashed box). Illustrating in different blue colors, the workspace lower limits

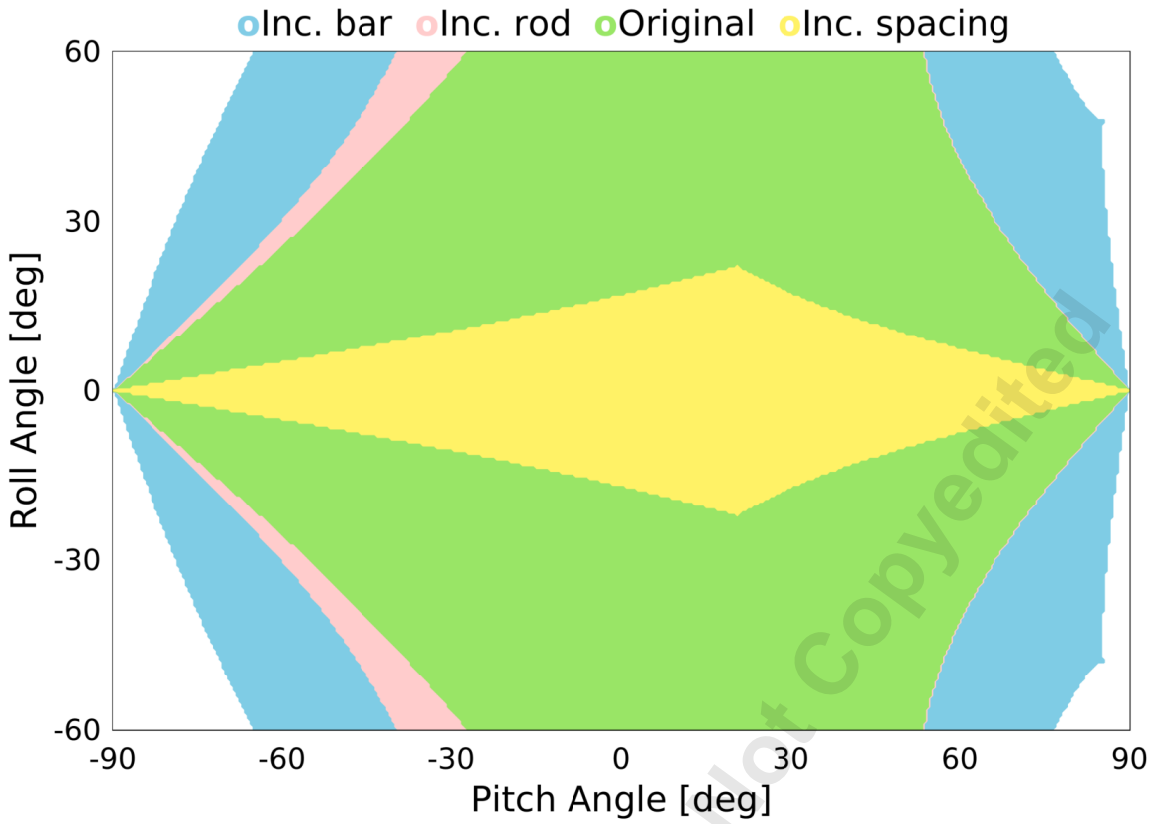

Fig. 4: The ankle workspaces w.r.t only the mechanism geometry, are illustrated in **green** for the default equal dimensions, in **blue** by increasing the motor bar length, in **pink** by increasing the rod length and in **yellow** by increasing the spacing between the two rods, respectively.

are generated with the motor lower limits of [-90, -80, -70, -64, -60] degree and the upper limits are generated with the motor upper limits of [90, 75, 60, 50, 40] degree, respectively. It can be seen that with minimum motor limits of [-64, 50] degree, the whole desired workspace is reachable. For a given desired ankle joint limits and limited size and volume of the tibia/ankle module, it is preferable to have minimum motor limits for the sake of mechanical simplicity during design stage. In addition, limited motor motion could also avoid potential unexpected collision/damage of the structure due to the unnecessary motions. Therefore, [-64, 50] degree are chosen as the motors limits for the proposed ankle module.

4 Experimental Verification

In this section, four experimental tests were carried out with the CogIMon tibia/ankle prototype module in order to validate the effectiveness of the proposed kinematics solvers. The first three tests demonstrated that the desired ankle workspace was reachable within the designed motor limits. The last test applied to a more practical task, that of the ankle motions required for walking with big steps.

The ankle joint references used for the four tests are separated by black dashed line shown in Fig. 6. The first test was a sinusoidal trajectory of roll joint with amplitude equal to the roll joint limit of 20 degree, whereas the pitch joint remained at zero position. The second test's reference for pitch joint consisted of two half sinusoidal wave with the amplitude equal to that of the pitch joint limits [-58, 42] degree, respectively, whereas the roll joint remained at zero position. The third test had the same pitch reference of the second test, but with the roll joint at its limit position, which is the exact top line of the red dashed box in Fig. 5.

For the forth test, we explored the humanoid motion control framework of Fig. 3 integrating with the proposed ankle kinematics solvers. First, the walking pattern considering the humanoid CogIMon's dimensions was generated by the pattern generator [21]. Then by solving the leg inverse kinematics [22], the ankle joint references were obtained. The walking pattern consisted of one 0.3 m forward step and one 0.2 m side step, which was a realistic gait for a biped whose leg length is around 0.8 m. From the right part of Fig. 6, one can also find that the humanoid CogIMon reserves the kinematic capability of performing larger steps.

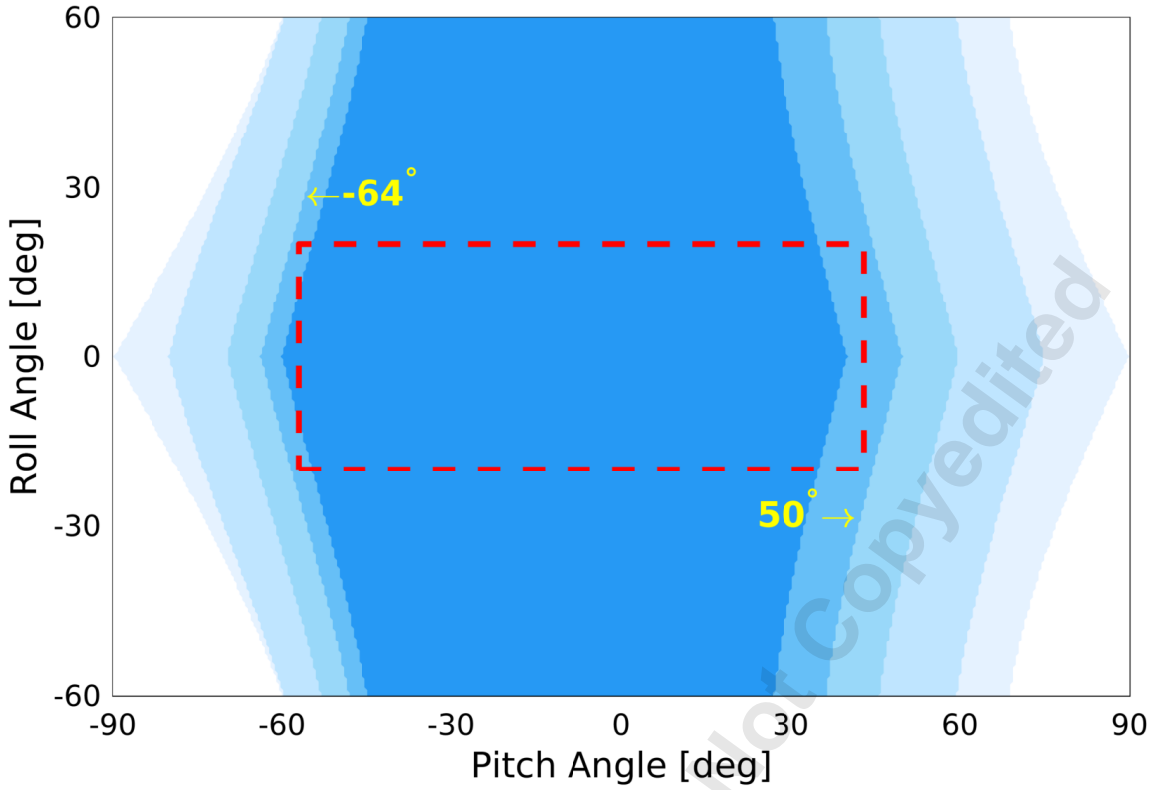

Fig. 5: The workspace of the proposed ankle illustrated by different motor limits with the lower limit varying from -90 to -60 degree and the upper limit varying from 90 to 40 degree. The red box represents the desired workspace. Therefore, the minimum required motor limits are [-64, 50] degree.

After the ankle joint references were obtained, the motor position references were solved by the ankle inverse kinematics and shown in Fig. 7. Note that the resolved motor positions were within the actuator limits of [-64, 50] degree. The accuracy of the proposed kinematics solvers was investigated by comparing the roll and pitch angle errors between the ankle joint references and the forward kinematics results using the motor positions in Fig. 7. The errors are shown in Fig. 8. They are smaller than $1e^{-6}$ degree during the whole experiment which indicates the exceptional accuracy of the proposed methods.

Meanwhile, the number of iterations for solving the forward kinematics using the Newton-Raphson method was no more than two during the tests as shown in Fig. 9. The average computational time for individual inverse kinematics was about $5e^{-7}$ s and the forward kinematics required more time as the number of iteration increased. However, the overall computational time tested on a laptop (Intel i7-4700HQ CPU) was still fast enough for real-time computation as shown in Fig. 10.

The snapshots of the experiment when the foot was at the limit positions are shown in Fig. 11.

5 Conclusion

This work contributes a comprehensive kinematics study and analysis for a humanoid ankle which is based on a 2-RSS-1-U spatial parallel mechanism. Mobility analysis of the parallel ankle mechanism was performed, using screw theory, for determining the number and properties of the mechanism's DoFs. Closed form solutions for the inverse kinematics and the Jacobian matrix are derived, and the forward kinematics is resolved numerically using the Newton-Raphson method. The workspace of the ankle joints is analyzed as part of the ankle module design process and the actuator limits are defined accordingly. Finally, an experimental validation was performed including four motion tests to evaluate the proposed analysis and kinematics solvers performance.

For the future work, we will mount the tibia on the CogIMon leg and investigate the advantages of the parallel mechanism in heavy-load locomotion scenarios. Joint torque and ankle impedance control will also be evaluated using the derived Jacobian matrix.

[4]Video of Fig. 11, `https://youtu.be/UsQDMN6KJnI`

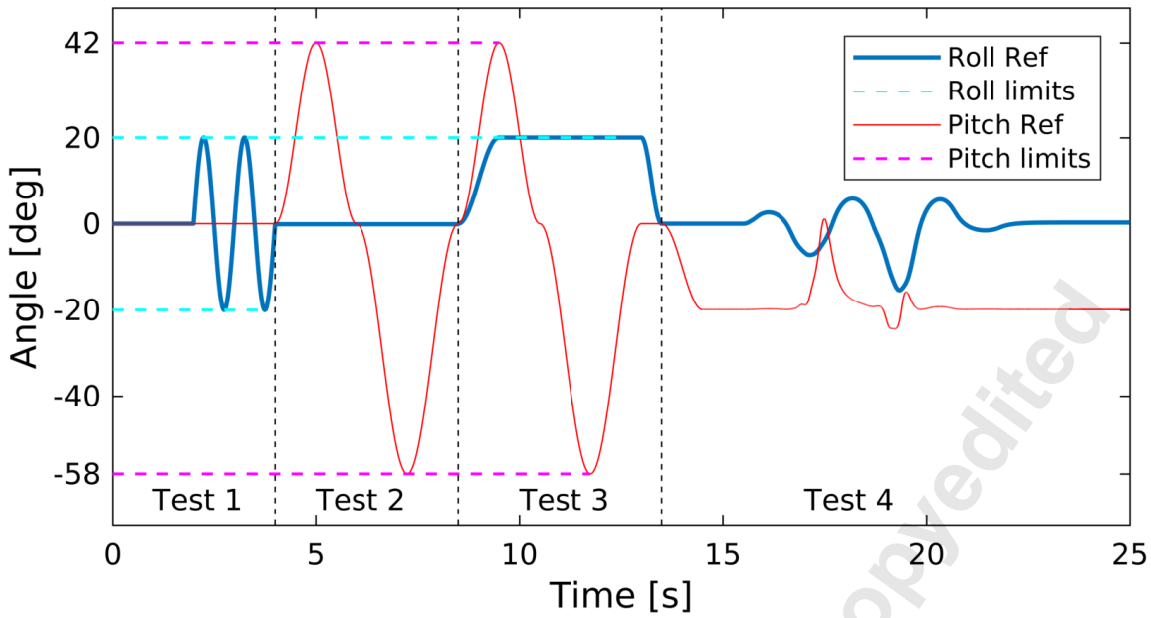

Fig. 6: Ankle joint references for the four experimental tests.

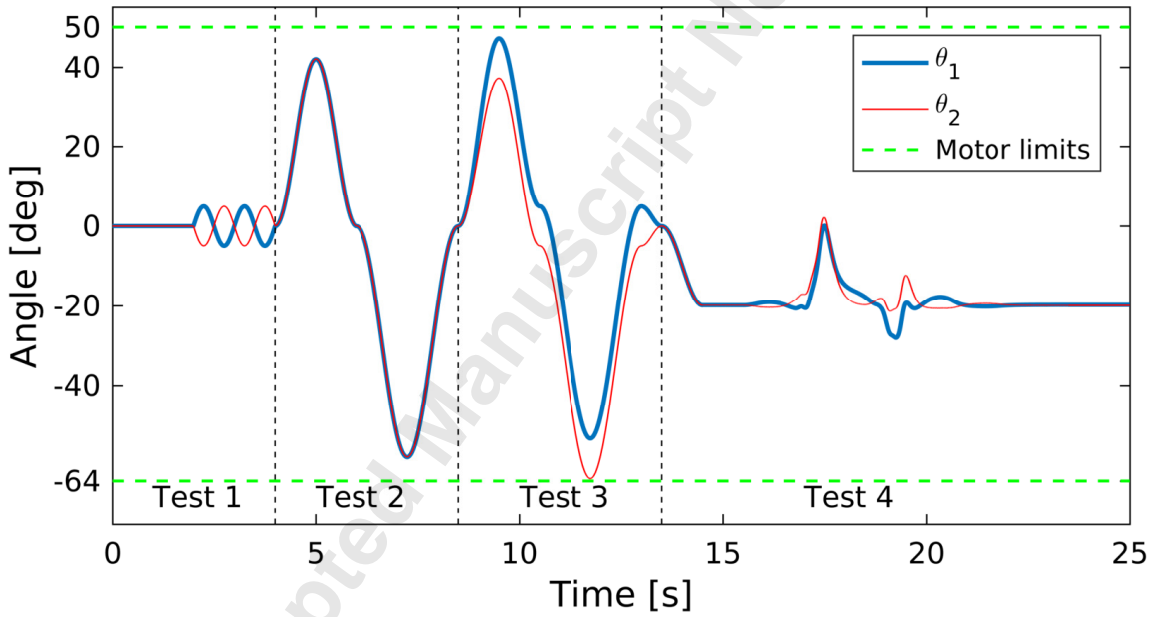

Fig. 7: Motor references solved by inverse kinematics for the four experimental tests.

Acknowledgment

The authors would like to acknowledge Francesco Di Dea for the mechanical design of the CogIMon robot. This work is supported by the European Union's Horizon 2020 robotics program CogIMon (ICT-23-2014, 644727)

References

[1] Lenarcic, J., and Stanisic, M., 2003. "A humanoid shoulder complex and the humeral pointing kinematics". *IEEE Transactions on Robotics and Automation,* **19**(3), pp. 499–506.

[2] Carricato, M., and Parenti-Castelli, V., 2004. "A novel fully decoupled 2-DOF parallel wrist". *The International Journal of Robotics Research,* **23**(6), pp. 661–667.

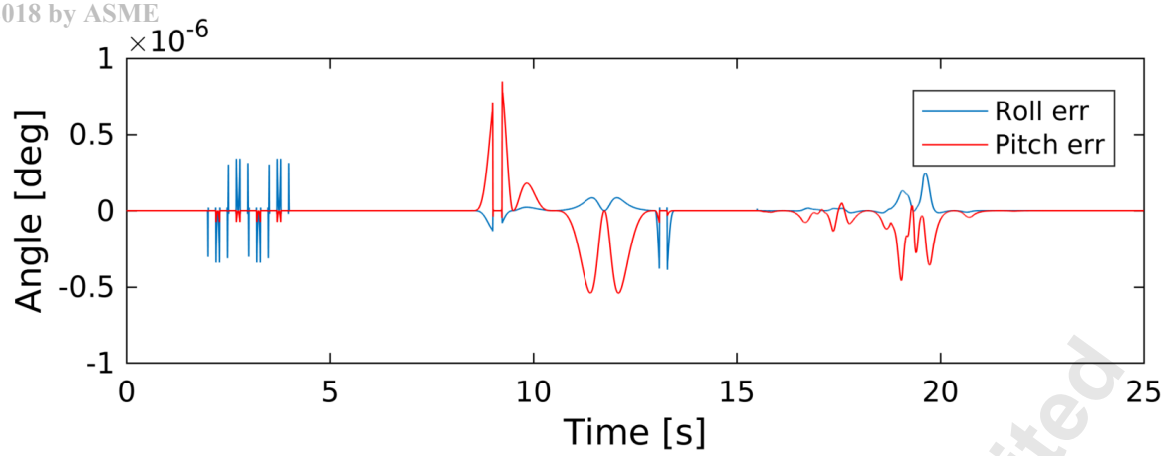

Fig. 8: Roll and pitch angle errors between the input references and the resultant ones after the IK-FK computation.

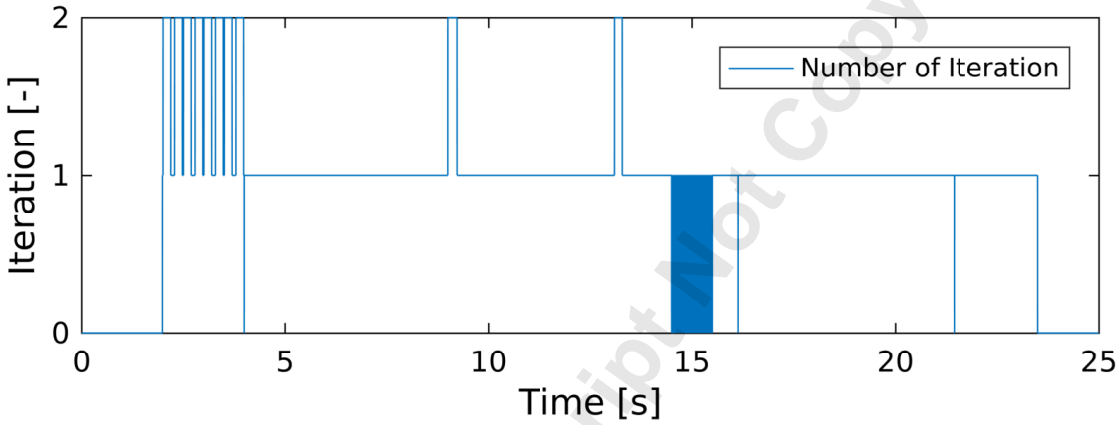

Fig. 9: Number of iterations for solving the forward kinematics during experiment.

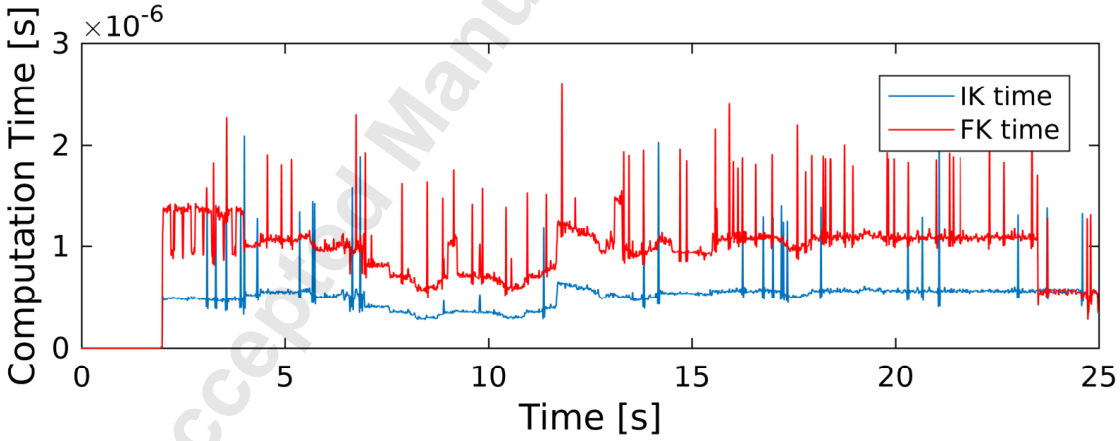

Fig. 10: Computational time of inverse and forward kinematics during experiment.

[3] Morisawa, M., Yakoh, T., Murakami, T., and Ohnishi, K., 2000. "An approach to biped robot with parallel mechanism". In International Workshop on Advanced Motion Control, pp. 537–541.
[4] Hashimoto, K., Sugahara, Y., Lim, H., and Takanishi, A., 2008. "Human-carrying biped walking vehicle". In International Conference of the International Society for Gerontechnology, Vol. 75.
[5] Saglia, J. A., Tsagarakis, N. G., Dai, J. S., and Caldwell, D. G., 2009. "A high-performance redundantly actuated parallel mechanism for ankle rehabilitation". *The International Journal of Robotics Research,* **28**(9), pp. 1216–1227.

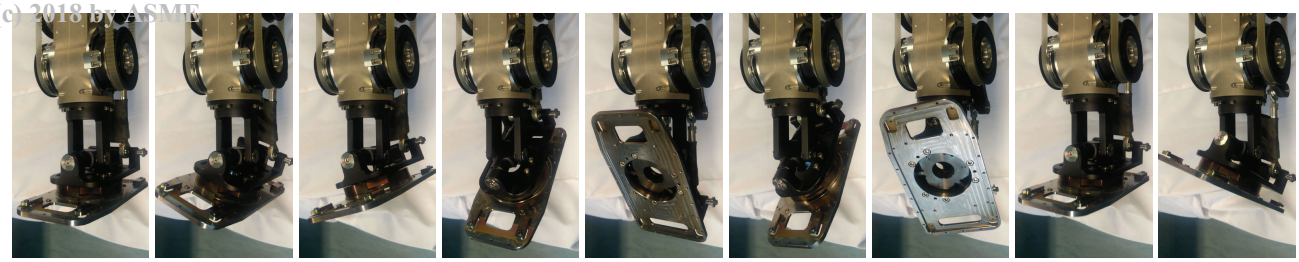

Fig. 11: Snapshots of the four experimental tests[4].

[6] Roy, A., Krebs, H. I., Williams, D. J., Bever, C. T., Forrester, L. W., Macko, R. M., and Hogan, N., 2009. "Robot-aided neurorehabilitation: a novel robot for ankle rehabilitation". *IEEE Transactions on Robotics,* **25**(3), pp. 569–582.

[7] Lohmeier, S., Buschmann, T., Schwienbacher, M., Ulbrich, H., and Pfeiffer, F., 2006. "Leg design for a humanoid walking robot". In IEEE-RAS International Conference on Humanoid Robots, pp. 536–541.

[8] Hyon, S.-H., Suewaka, D., Torii, Y., and Oku, N., 2017. "Design and experimental evaluation of a fast torque-controlled hydraulic humanoid robot". *IEEE/ASME Transactions on Mechatronics,* **22**(2), pp. 623–634.

[9] Feng, S., Xinjilefu, X., Atkeson, C. G., and Kim, J., 2015. "Optimization based controller design and implementation for the atlas robot in the darpa robotics challenge finals". In IEEE-RAS International Conference on Humanoid Robots, pp. 1028–1035.

[10] Kaminaga, H., Ko, T., Masumura, R., Komagata, M., Sato, S., Yorita, S., and Nakamura, Y., 2016. "Mechanism and control of whole-body electro-hydrostatic actuator driven humanoid robot Hydra". In International Symposium on Experimental Robotics, pp. 656–665.

[11] Knabe, C., Griffin, R., Burton, J., Cantor-Cooke, G., Dantanarayana, L., Day, G., Ebeling-Koning, O., Hahn, E., Hopkins, M., Neal, J., et al., 2017. "Team VALOR's ESCHER: A novel electromechanical biped for the DARPA robotics challenge". *Journal of Field Robotics,* **34**(5), pp. 912–939.

[12] Kakiuchi, Y., Kamon, M., Shimomura, N., Yukizaki, S., Takasugi, N., Nozawa, S., Okada, K., and Inaba, M., 2017. "Development of life-sized humanoid robot platform with robustness for falling down, long time working and error occurrence". In IEEE/RSJ International Conference on Intelligent Robots and Systems, pp. 689–696.

[13] Reher, J., Cousineau, E. A., Hereid, A., Hubicki, C. M., and Ames, A. D., 2016. "Realizing dynamic and efficient bipedal locomotion on the humanoid robot DURUS". In IEEE International Conference on Robotics and Automation, pp. 1794–1801.

[14] Mazumdar, A., Spencer, S. J., Hobart, C., Salton, J., Quigley, M., Wu, T., Bertrand, S., Pratt, J., and Buerger, S. P., 2017. "Parallel elastic elements improve energy efficiency on the STEPPR bipedal walking robot". *IEEE/ASME Transactions on Mechatronics,* **22**(2), pp. 898–908.

[15] Han, S., Um, S., and Kim, S., 2016. "Mechanical design of robot lower body based on four-bar linkage structure for energy efficient bipedal walking". In IEEE International Symposium on Safety, Security, and Rescue Robotics, pp. 402–407.

[16] Alfayad, S., Ouezdou, F. B., and Namoun, F., 2009. "New three DoF ankle mechanism for humanoid robotic application: Modeling, design and realization". In IEEE/RSJ International Conference on Intelligent Robots and Systems, pp. 4969–4976.

[17] Huang, Z., and Li, Q., 2003. "Type synthesis of symmetrical lower-mobility parallel mechanisms using the constraint-synthesis method". *The International Journal of Robotics Research,* **22**(1), pp. 59–79.

[18] Hunt, K. H., 1978. *Kinematic geometry of mechanisms*. Oxford University Press.

[19] Murray, R. M., Li, Z., Sastry, S. S., and Sastry, S. S., 1994. *A mathematical introduction to robotic manipulation*. CRC press.

[20] Dai, J. S., Huang, Z., and Lipkin, H., 2006. "Mobility of overconstrained parallel mechanisms". *Journal of Mechanical Design,* **128**(1), pp. 220–229.

[21] Zhou, C., Wang, X., Li, Z., and Tsagarakis, N., 2017. "Overview of Gait Synthesis for the Humanoid COMAN". *Journal of Bionic Engineering,* **14**(1), pp. 15–25.

[22] Zhou, C., Fang, C., Wang, X., Li, Z., and Tsagarakis, N., 2016. "A Generic Optimization-based Framework for Reactive Collision Avoidance in Bipedal Locomotion". In IEEE Conference on Automation Science and Engineering, pp. 1026–1033.

[23] Tsai, M.-S., Shiau, T.-N., Tsai, Y.-J., and Chang, T.-H., 2003. "Direct kinematic analysis of a 3-PRS parallel mechanism". *Mechanism and Machine Theory,* **38**(1), pp. 71–83.

List of Tables

1 Example of solving the forward kinematics using Newton-Raphson method (unit: degree), the motor references are $[-46.38490723; -53.91584432]$ degree. 8
2 The workspace changes w.r.t the linkage dimensions according to Fig. 4. 8

List of Figures

1 Mechanical model of the CogIMon humanoid robot (left) and close back view of its tibia without covers (right). 2
2 The ankle's schematic representation. 3
3 Typical Control Framework for humanoid motion control. The superscript *m* indicates the variable is measured by the sensors. 6
4 The ankle workspaces w.r.t only the mechanism geometry, are illustrated in **green** for the default equal dimensions, in **blue** by increasing the motor bar length, in **pink** by increasing the rod length and in **yellow** by increasing the spacing between the two rods, respectively. 9
5 The workspace of the proposed ankle illustrated by different motor limits with the lower limit varying from -90 to -60 degree and the upper limit varying from 90 to 40 degree. The red box represents the desired workspace. Therefore, the minimum required motor limits are [-64, 50] degree. 10
6 Ankle joint references for the four experimental tests. 11
7 Motor references solved by inverse kinematics for the four experimental tests. 11
8 Roll and pitch angle errors between the input references and the resultant ones after the IK-FK computation. 12
9 Number of iterations for solving the forward kinematics during experiment. 12
10 Computational time of inverse and forward kinematics during experiment. 12